Molecular and Cellular Endocrinology 564 (2023) 111868

Contents lists available at ScienceDirect

Molecular and Cellular Endocrinology

journal homepage: www.elsevier.com/locate/mce

Developmental programming: Adipose depot-specific regulation of non-coding RNAs and their relation to coding RNA expression in prenatal testosterone and prenatal bisphenol-A -treated female sheep☆

John Dou [a,1], Soundara Viveka Thangaraj [b,1], Muraly Puttabyatappa [b], Venkateswaran Ramamoorthi Elangovan [b], Kelly Bakulski [a,**], Vasantha Padmanabhan [b,*]

[a] Department of Epidemiology, University of Michigan, Ann Arbor, MI, USA
[b] Department of Pediatrics, University of Michigan, Ann Arbor, MI, USA

ARTICLE INFO

Handling Editor: Carolyn M. Klinge

Keywords:
Fetal programming
Endocrine disruptors
RNA sequencing
Steroids
Insulin resistance

ABSTRACT

Inappropriate developmental exposure to steroids is linked to metabolic disorders. Prenatal testosterone excess or bisphenol A (BPA, an environmental estrogen mimic) leads to insulin resistance and adipocyte disruptions in female lambs. Adipocytes are key regulators of insulin sensitivity. Metabolic tissue-specific differences in insulin sensitivity coupled with adipose depot-specific changes in key mRNAs, were previously observed with prenatal steroid exposure. We hypothesized that depot-specific changes in the non-coding RNA (ncRNA) - regulators of gene expression would account for the direction of changes seen in mRNAs. Non-coding RNA (lncRNA, miRNA, snoRNA, snRNA) from various adipose depots of prenatal testosterone and BPA-treated animals were sequenced. Adipose depot-specific changes in the ncRNA that are consistent with the depot-specific mRNA expression in terms of directionality of changes and functional implications in insulin resistance, adipocyte differentiation and cardiac hypertrophy were found. Importantly, the adipose depot-specific ncRNA changes were model-specific and mutually exclusive, suggestive of different regulatory entry points in this regulation.

1. Introduction

Developmental insults contribute to increases in non-communicable diseases, including cardiovascular diseases (CVD), diabetes mellitus (DM), and several cancers (Barouki et al., 2012; Zarean and Poursafa, 2019; Kumar et al., 2020). Inappropriate exposure to endogenous steroids or environmental steroid mimics serves as one such insult (Abruzzese et al., 2018; Puttabyatappa et al., 2017), that is known to program the metabolic axis (Cardoso and Padmanabhan, 2019).

Our studies with sheep demonstrated prenatal exposure to testosterone (T)- an endogenous steroid or bisphenol A (BPA)- an environmental steroid-mimic, produces reproductive and metabolic perturbations that are characteristic of polycystic ovary syndrome-like phenotype in the female offspring (T (Padmanabhan and Veiga-Lopez, 2013); BPA (Veiga-Lopez et al., 2016; Padmanabhan et al., 2010)), albeit the phenotype is less severe in the BPA model. At the metabolic level, both prenatal T (Ferreira et al., 2021; Puttabyatappa and Padmanabhan, 2017) and BPA (Veiga-Lopez et al., 2016; Puttabyatappa et al., 2019)) models manifested insulin resistance and adipocyte dysfunctions (T (Cardoso et al., 2016); BPA (Veiga-Lopez et al., 2016)). Specifically, prenatal exposure to excess T, an estrogen precursor, induced dyslipidemia, peripheral insulin resistance, ectopic lipid accumulation, and an increase in the distribution of small adipocytes in female offspring (Veiga-Lopez et al., 2013a). Prenatal exposure to BPA, a xenoestrogen with estrogenic action, induced insulin resistance, adipocyte hypertrophy and adipose depot-specific disruptions in markers of

☆ Research reported in this publication was supported by Eunice Kennedy Shriver National Institute of Child Health & Human Development, National Institutes of Health (NIH) under award R01HD099096 and P01 HD44232, and National Institute of Environmental Health Sciences R01 ES016541, R01 ES 030374, and P30 ES017885. MP was supported via Ruth L. Kirschstein Institutional Training Grant T32 ES007062. TSV is a Center Scientist in M-LEEaD NIEHS Core Center P30 ES017885.

* Corresponding author. Department of Pediatrics, University of Michigan, 7510 MSRB 1, 1500 W. Medical Center Drive, Ann Arbor, MI, 48109, USA.
** Corresponding author. Department of Epidemiology, M5511 SPH II, Ann Arbor, MI, 48109, USA.
E-mail addresses: bakulski@umich.edu (K. Bakulski), vasantha@umich.edu (V. Padmanabhan).
[1] Share equal credit.

https://doi.org/10.1016/j.mce.2023.111868
Received 14 December 2022; Received in revised form 19 January 2023; Accepted 22 January 2023
Available online 26 January 2023

adipose differentiation in female offspring.

Adipose tissue, composed of adipocytes, is primarily a fuel reservoir that also serves as an endocrine organ, secreting several adipokines that regulate other metabolic tissues like muscle, liver and pancreas. Recent research has established the role of adipose tissue as a dominant regulator of glucose homeostasis and whole-body metabolism (Luo and Liu, 2016; Maliszewska and Kretowski, 2021). The role of adipose depot as a major contributor to insulin resistance (Kim et al., 2015) is underlined by the observation that both excess of adipose, as seen in obesity (Koenen et al., 2021) and deficiency of adipose, as seen in lipodystrophy (Patni and Garg, 2022) can lead to development of insulin resistance. Similarly, aberrant changes in adipocyte differentiation such as increased adipocyte size is also associated with the development of insulin resistance (Stenkula and Erlanson-Albertsson, 2018). Because adipose tissues are compartmentalized into discrete depots and distributed throughout the body, there are functional depot-specific differences in their influence of tissue-specific insulin resistance (Luong et al., 2019). Subcutaneous adipose tissue (SAT), the fat beneath the skin and visceral adipose tissue (VAT), the intra-abdominal fat, form the major adipose depots of the body. While SAT favors uptake and storage of lipids and is associated with a metabolically healthy phenotype, VAT promotes lipid turnover and is associated with cardiometabolic disorders (Arner and Ryden, 2022). The smaller depots that are associated with specific organ systems such as the epicardiac adipose tissue (ECAT) and perirenal adipose tissue (PRAT) can influence the organs in their proximity (Lee et al., 2013). Perturbations in ECAT are associated with obesity-related insulin resistance (Iacobellis and Leonetti, 2005), a risk factor for cardiovascular diseases (Russo et al., 2018) while disruption in PRAT is associated with cardiovascular diseases and chronic kidney disease risk (Huang et al., 2020; Liu et al., 2019).

Knowledge of adipose depot-specific changes in gene transcription and their regulation are therefore much needed to delineate the roles they play in eliciting organ-specific changes in insulin sensitivity. Our recent studies with prenatal T-treated animals demonstrated adipose depot-specific transcriptional changes manifested as increased proinflammatory genes in VAT, reduced adipocyte differentiation genes in VAT and SAT, increased cardiomyocyte function gene expression in ECAT, and increased vascular related gene expression in PRAT (Dou et al., 2021a). Our studies with prenatal BPA-treated sheep, which focused only on VAT and SAT, found increased expression of genes involved in adipocyte development and differentiation and thermogenic brown/beige adipocyte development in the SAT, while in VAT proinflammatory genes and genes involved in adipogenesis and maintenance of insulin sensitivity were upregulated (Dou et al., 2020). While these results from prenatal steroid (endogenous or environmental)-treated models demonstrate depot-specific regulation, the mechanisms by which these changes are facilitated is unknown.

Non-coding RNAs (ncRNA) like long non-coding RNA (lncRNA) and microRNA (miRNA) exert epigenetic control by regulating gene expression at the transcriptional and post-translational levels and serve as sensors of environmental insults (Wei et al., 2017). Dysregulation of lncRNA (Wang et al., 2021; Luo et al., 2016; Huang et al., 2018) and miRNA (Li et al., 2019) are important regulators of the pathological response to environmental exposures. Some lncRNAs are important regulators in adipogenesis and adipocyte metabolism and several miRNAs have been implicated in metabolic diseases (Agbu and Carthew, 2021). Small nuclear RNA (snRNA) are involved in regulating gene expression by splicing (Li et al., 2021) while small nucleolar RNA (snoRNA) guide posttranscriptional modifications on ribosomal RNA and snRNA (Bratkovič et al., 2020). snRNA and snoRNA are largely unexplored but are gaining importance for their potential role in adipogenesis and metabolic health (Chao et al., 2021, 2022). Given the emerging role of ncRNA in metabolic homeostasis, we hypothesized that prenatal exposure to excess T (an endogenous androgen) or BPA (an environmental estrogen-mimic) will induce steroid and adipose depot-specific disruptions in the ncRNA landscape that are consistent with the reported transcriptomic and phenotypic outcomes.

2. Methods

2.1. Animals

Animal studies were conducted at the University of Michigan Sheep Research Facility (Ann Arbor, MI) using multiparous female Suffolk sheep. Studies were conducted following Institutional Animal Care and Use Committee of the University of Michigan approved protocol that met the requirements of the National Research Council's Guide for the Care and Use of Laboratory Animals and the Animal Welfare Act. Two cohorts of sheep were included in this study, one examining the effects of prenatal T treatment, and one examining effects of prenatal BPA treatment. Animals from both cohorts (Cohort 1: control and prenatal T-treated; Cohort 2: control and prenatal BPA-treated) were co-inhabited under similar conditions, fed a similar maintenance diet to prevent obesity, and potential phytoestrogen exposure via diet was similar across treatment groups as described earlier (Manikkam et al., 2004).

2.2. Prenatal T treatment

Between gestational days 30–90, which is the sexually dimorphic window when fetal males see an increase in testosterone naturally, 100 mg T propionate (~1.2 mg/kg; Millipore Sigma, St. Louis, MO) suspended in corn oil was administered intramuscularly twice a week to the prenatal T-treated Suffolk sheep. Control animals did not receive any vehicle treatment, since our prior studies demonstrated no effects of corn oil in sheep (Veiga-Lopez et al., 2008). From this cohort, four control and prenatal T-treated female sheep ensuring mother as the experimental unit were randomly selected for the current study. The effects of prenatal T-treatment on peripheral insulin sensitivity, adiposity, tissue specific changes in mediators of insulin sensitivity and transcriptome analysis of coding RNA from this cohort have been published (Puttabyatappa et al., 2017, 2018, 2020; Cardoso et al., 2016; Lu et al., 2016).

2.3. Prenatal BPA treatment

Pregnant Suffolk sheep were randomly assigned to control and BPA treatment groups. Between days 30 and 90 of gestation, which is the sexually dimorphic window, control animals received vehicle (corn oil) and the BPA-treated group received 0.5 mg/kg/day BPA (purity ≥99%, catalog number 239658; Aldrich Chemical Co, Milwaukee, Wisconsin) solubilized in corn oil (Veiga-Lopez et al., 2013b). Both injections of vehicle and BPA were administered daily, subcutaneously. The average BPA level achieved in the umbilical artery with this dose was ~2.6 ng/ml (Veiga-Lopez et al., 2013b) and this concentration is within the range reported in human biomonitoring studies (Gerona et al., 2013; Lee et al., 2018; Veiga-Lopez et al., 2015a). From this cohort, four control and prenatal BPA-treated female sheep, ensuring mother as the experimental unit, were randomly selected, and used in the current study. The effects of prenatal BPA-treatment on insulin sensitivity, adiposity, mediators of insulin sensitivity and transcriptome analysis of coding RNA from this cohort have been previously published (Veiga-Lopez et al., 2015b, 2016; Puttabyatappa et al., 2019).

2.4. Tissue collection

Animals from the T cohort were ovariectomized at the end of the second breeding season to remove confounding effects from differing steroid background. For this cohort, adipose depot samples were collected during the artificial follicular phase, as described previously (Puttabyatappa et al., 2017). Early follicular phase levels of estradiol was achieved by inserting a 1 cm estradiol implant subcutaneously (Goodman et al., 1981). An artificial luteal phase of the estrus cycle was

initiated by placing two controlled internal drug-releasing implants containing progesterone (CIDR-G; InterAg, Hamilton, New Zealand) subcutaneously. After 14 days, progesterone implants were removed, four 30-mm estradiol implants inserted subcutaneously to mimic follicular phase and 18 h later animals were euthanized by barbiturate overdose (Fatal Plus; Vortech Pharmaceuticals, Dearborn, MI) and tissues collected. Tissues from the prenatal BPA-treated cohort were collected from animals euthanized by barbiturate overdose during natural follicular phase following synchronization with two injections of PGF2a administered 11 days apart (27h after administration of second PGF2a). In the prenatal T cohort, four adipose depots were collected: VAT from the omental fat surrounding the ventral sac of the rumen, SAT from under the skin in the sternal region, PRAT from around the kidney, and ECAT from between the myocardium and the serous/visceral layer. In the prenatal BPA cohort, only SAT and VAT were collected. (Supplementary Table S1). Samples were immediately flash-frozen and stored at −80 °C.

2.5. RNA extraction, library construction and sequencing

Adipose tissue was homogenized with liquid nitrogen and dissolved in Trizol reagent (Life Technologies, Carlsbad, CA) and total RNA isolated as per manufacturer's recommendations. Residual DNA was removed using the RNeasy binding column, treating with RNAse free DNAse (Qiagen, Germantown, MD) then eluting RNA in nuclease free water. RNA purity and integrity were measured with the Agilent 2100 bioanalyzer (Agilent Technologies, Santa Clara, CA). Libraries for ncRNA were prepared using the NEBNext smallRNA kit (New England BioLabs, Ipswich, MA) at the University of Michigan Advanced Genomics Core as per manufacturer's recommendations. Sequencing was performed on an Illumina Nextseq platform.

2.6. Data processing and quality control

First, raw fastq files were 5′ trimmed with cutadapt (v3.2) (Martin, 2011) to remove the adapter sequence 'AGATCGGAAGAGCACACGTCTGAACTCCAGTCAC' as per manufacturer's recommendation. Additionally, reads that were of low quality and <17bps were removed from the sequencing data. FastQC (v0.11.5) (Andrews, 2010) was performed on both the raw and trimmed reads, with reports summarized using MultiQC (Ewels et al., 2016). The trimmed reads were aligned to the sheep reference genome (Oar_rambouillet_v1.0) using the Spliced Transcripts Alignment to a Reference (STAR) program (v2.6.0c) (Dobin et al., 2013). Quality metrics of reads mapped to the genome were evaluated using Quality of RNA-Seq Tool-Set (QoRTS, v1.3.6) software (Hartley and Mullikin, 2015). FeatureCounts (v1.6.1) software (Liao et al., 2014) was used to count the number of reads of each ncRNA. For featureCounts, annotation files were subset to each class of ncRNA (miRNA, lncRNA, snRNA, and snoRNA). Subsequent analyses were stratified by class of ncRNA.

2.7. Differential RNA expression

Differential expression of ncRNAs were evaluated using the DESeq2 (v1.24.0) package in R statistical software, which performs linear regression modeling counts on a negative binomial distribution (Love et al., 2014). Normalization was done with default package settings. To evaluate similarity between the prenatal T cohort and the BPA cohort (artificial follicular phase vs. natural follicular phase), we compared expression levels between the SAT and VAT samples of the control animals across the two cohorts. To evaluate adipose depot-specific differences, control samples of each tissue type were compared against all the other tissue types within cohorts. In both cohorts, we examined differential impact of treatment stratified by adipose tissue types [4 adipose types in prenatal T (VAT, SAT, ECAT and PRAT) and 2 adipose types in prenatal BPA cohorts (VAT and SAT)]. Analysis was done separately for the prenatal BPA data and the prenatal T data, in addition to stratification by ncRNA class. The differentially expressed ncRNA for each evaluation was visualized using the EnhancedVolcano package (Blighe et al., 2021). Univariate analysis using volcano plots with cut-off value of adjusted p-value <0.05 and absolute log-fold change >0.5 was used to identify the significant ncRNA.

2.8. Multivariate analysis

Data reduction was done using SIMCA version 17 (Umetrics, Umea, Sweden) software. Multivariate modeling was applied to the imported normalized counts for ncRNA from adipose tissues. Unsupervised principal component analysis (PCA) was performed to get an overview of the data and identify potential outliers and trends in the data. The principal components (PC) were displayed in two-dimensional and three-dimensional score plots to allow visualization of the distribution and grouping of the samples. Hoteling's T-square statistic, a multivariate extension of the Student's t-test, was employed to draw a tolerance ellipse around the sample cluster and any data outside the ellipse was considered outliers. No outliers were found in the data sets.

Differences between control and treatment groups were visualized using the supervised approach of orthogonal projections to latent structure discriminant analysis (OPLS-DA) using SIMCA version 17 software (Umetrics, Umea, Sweden). The variations arising from treatment were the first predictive component and variations not related to treatment were explained by the orthogonal components. In this model, the status of treatment (control and prenatal T or BPA) was the outcome (Y) variable, and the ncRNA expression data was the predictor (X) variable and association between these are highlighted by filtering the orthogonal variation. The differences in the transcriptome profiles were summarized in the OPLS-DA score plots that were developed for the first predictive component and the first orthogonal component and each point on the score plot represents one animal. Q^2 and R^2 values indicate the robustness of the model with values above 0.5 indicating a good model. The generated OPLS-DA models were validated using a 100-iteration permutation test to avoid over-fitting and false-positives. The model was considered valid if all Q^2 values from the permuted data set are lower than the Q^2 values on the actual dataset. The variables of importance in projection (VIP) scores reflect the contribution of the ncRNA to the model and a cut-off of VIP>1 was used in this study.

2.9. Correlation between ncRNA and coding RNA

Data on coding RNA from the same samples have been previously published (Dou et al., 2020, 2021b). We matched ncRNA from the current study with this previous data. The Differential Gene Correlation Analysis (DGCA) package (McKenzie et al., 2016) was used to determine putative ncRNA-mRNA pairs. As an exploratory analysis liberal cutoff criteria were used for consideration in analysis. Any ncRNA with adjusted p-value <0.1 in the current study, and coding RNA from the previously published studies with adjusted p-value <0.1 and absolute log fold change >1.0 were evaluated using correlation matrices. Among these ncRNA and mRNA, ncRNA-mRNA pairs that met the Pearson correlation coefficients with p-values <0.05 across control and treatment groups were retained and visualized. Box plots for the gene expression levels were generated using the web tool BoxPlotR (Spitzer et al., 2014).

2.10. Data and code availability

The new ncRNA sequencing data are publicly available through the National Institutes of Health's Genome Expression Omnibus (https://www.ncbi.nlm.nih.gov/geo/; accession number GSE219111). The re-analyzed coding RNA sequencing data remain publicly available through the Genome Expression Omnibus (accession numbers: GSE158436 for T-treatment and GSE142222 for BPA-treatment). Code

to conduct the current analysis is publicly available through GitHub (https://github.com/bakulskilab/Developmental-Programming-adipose-depot-specific-regulation-of-non-coding-RNAs).

3. Results

3.1. Adipose tissue-specific differential expression in controls

The total number of non-coding RNA identified in the control vs. treatment groups of prenatal T-treated BPA-treated cohorts are listed in Supplementary Table S2. Comparison of ncRNA expression across the four adipose depot types in control samples from the prenatal T-model found VAT to be the least distinct, when compared to the other three adipose types, with no ncRNA reaching significance. Also, snRNA patterns were not significantly different among the other three adipose depot types (Fig. 1, left panel). In contrast, expression levels of lncRNA, miRNA, and snoRNA in ECAT, PRAT, and SAT differed from the other three adipose types. Differential expression analysis results from all depots of prenatal T cohort are included in Supplementary Table S3. Comparison of ncRNA profiles in the SAT and VAT depots in controls from the prenatal BPA-model identified 9 lncRNAs, 25 miRNAs, 45 snoRNAs and 2 snRNAs that were differentially expressed between these two depots (Fig. 1, right panel). Differential expression analysis results for SAT and VAT comparison in the prenatal BPA cohort are listed in Supplementary Table S4.

3.2. Prenatal-T treatment effect

The effect of prenatal T-treatment in each adipose depot is discussed below by ncRNA class. Differential expression analysis in ECAT identified ten significant miRNAs. Specifically, prenatal T-treatment increased the expression of six miRNAs (*miR-99A, miR-10B, miR-143, miR-3959, miR-199A, and miR-218A*), while decreasing expression of four other miRNA (*miR-150, miR-485, miR-433, and miR-543*) in ECAT. In PRAT, prenatal T-treatment decreased the expression of the miRNA, *miR-133*. In VAT, prenatal-T treatment increased the expression of the miRNA, *miR-3955* and four snoRNA (*LOC114117654, LOC114110216* and *LOC114110211* of the SNORA18 family *and LOC114112592*) (Fig. 2).

Multivariate analysis identified overall T-treatment specific differences based on ncRNA class. Although unsupervised PCA on the first two dimensions did not show clear separation between the control and T-treatment, the 3-D PCA score plot showed clear clustering of the control samples in miRNA, snRNA and snoRNA in the ECAT and miRNA in PRAT (Fig. 3). This was also confirmed by the supervised OPLS-DA models

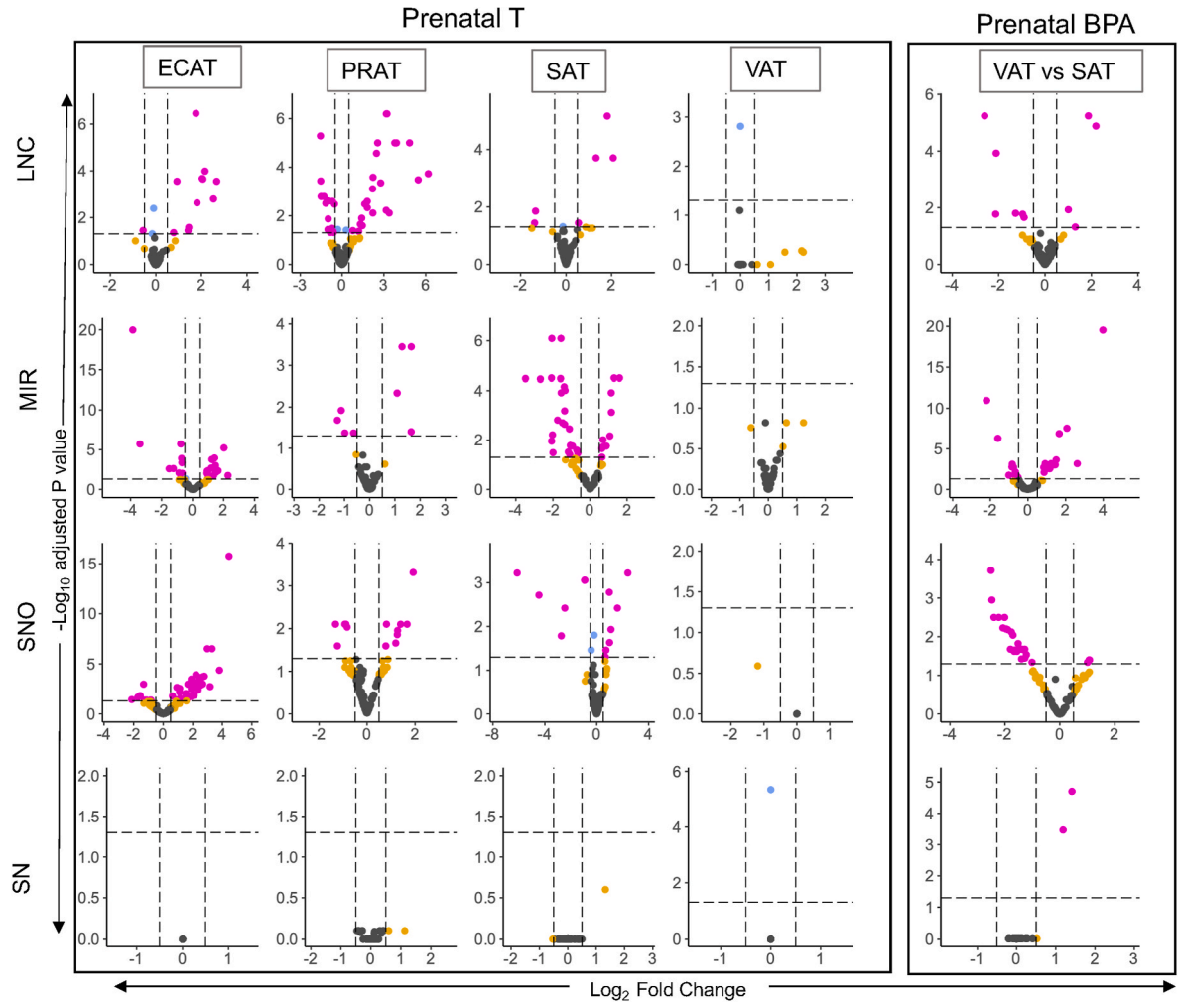

Fig. 1. Differential expression of ncRNAs in adipocyte tissue types in controls. Volcano plot representation of differential expression of lncRNA, miRNA, snoRNA, and snRNA in ECAT, PRAT, SAT and VAT of the prenatal T-treated cohort is represented in the left panel and that between SAT and VAT in the prenatal -BPA-treated cohort in the right panel. ncRNA are plotted by $\log_2$ fold change on the x-axis and $-\log_{10}$ adjusted P values on the y-axis. Pink points represent the genes that have an absolute $\log_2$ fold change greater than 0.5 and adjusted P values less than 0.05. Yellow dots represent genes that met the absolute $\log_2$ fold change greater than 0.5 but did not meet the *P*-adjusted cutoff of less than 0.05, blue dots represent genes that met *P*-adjusted cutoff of less than 0.05 but did not meet absolute $\log_2$ fold change greater than 0.5. Grey dots represent genes that did not meet either cutoff criterion.

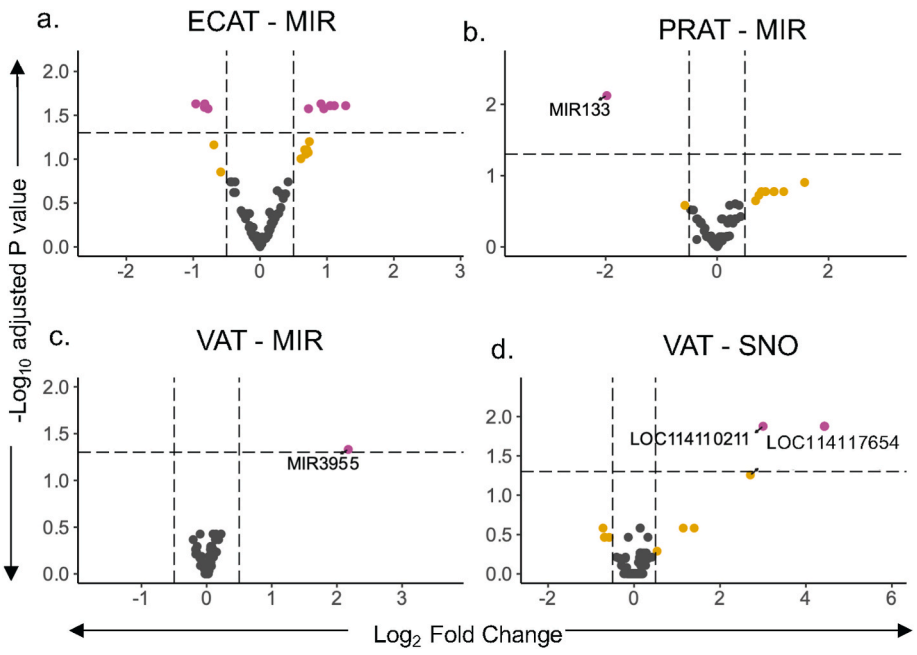

Fig. 2. Prenatal -T treatment related differential expression of ncRNA by adipose tissue type: Volcano plot representation of differential expression. a. miRNA in ECAT, b. miRNA in PRAT, c. miRNA in VAT, and d. snoRNA in VAT. ncRNA are plotted by $\log_2$ fold change on the x-axis and $-\log_{10}$ *P* adjusted values on the y-axis. Pink points represent the genes that have an absolute $\log_2$ fold change greater than 0.5 and *P* adjusted values less than 0.05. Grey dots represent genes that did not meet *P*-adjusted cutoff of less than 0.05 and absolute $\log_2$ fold change greater than 0.5 and yellow dots represent genes that met the absolute $\log_2$ fold change greater than 0.5 but did not meet the *P*-adjusted cutoff of less than 0.05.

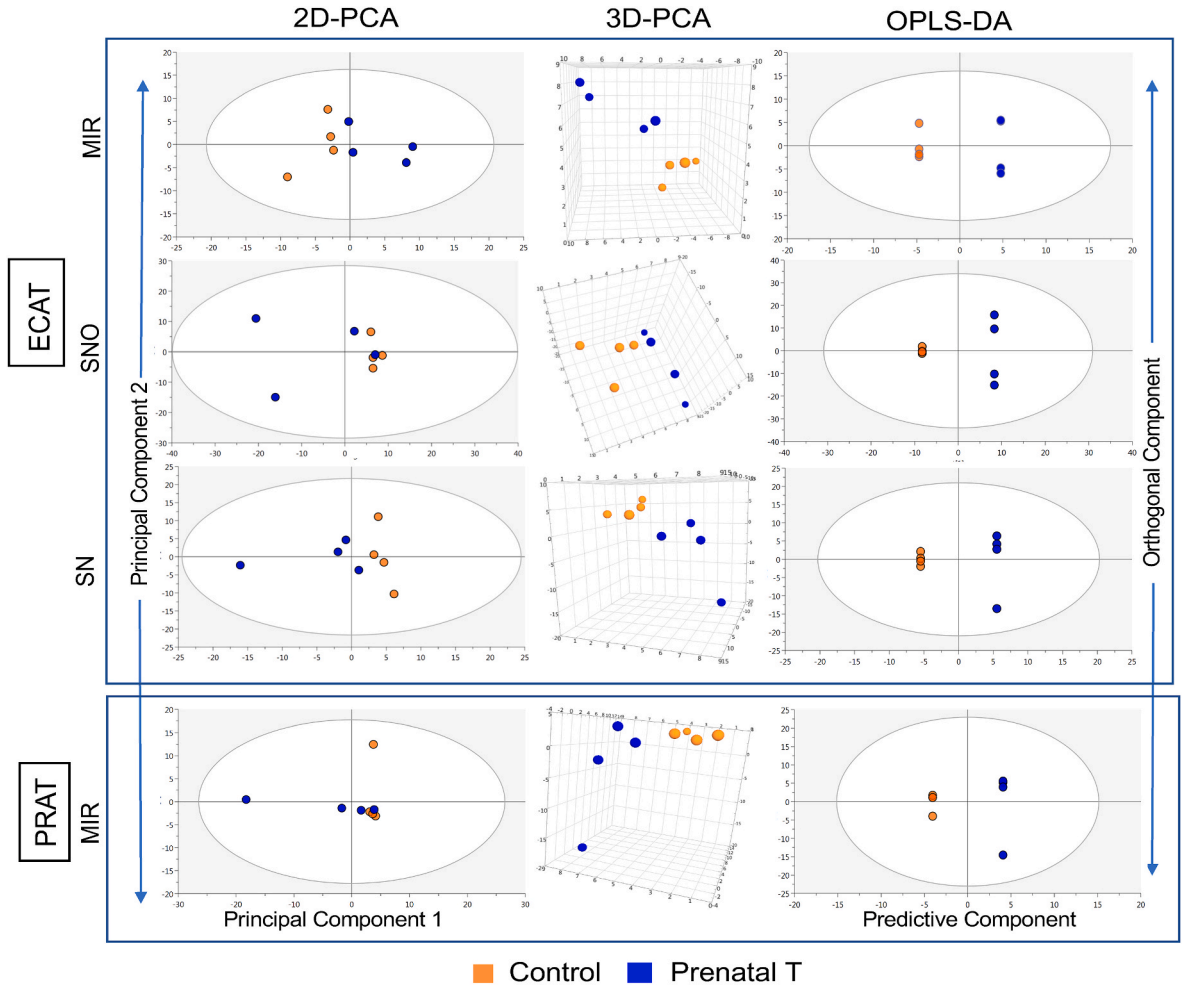

Fig. 3. Overall patterns of ncRNA expression in ECAT and PRAT in response to prenatal T-treatment: PCA analysis - 2D and 3D score plots and Orthogonal projections to latent structure discriminant analysis (OPLS-DA) score plots on miRNA, snoRNA and snRNA.

with R^2 and Q^2Y values above 0.6 indicating a robust model and validated by a permutation test. SAT did not show a separation of samples based on treatment in any of the ncRNA classes (Fig. 4-left panel). miRNA and snoRNA in VAT showed separation between the control and prenatal T-treated groups, based on validated OPLS-DA models (Fig. 4 – right panel). Other tissues and ncRNA classes did not meet significance (Supplementary Fig. S1). Table 1 lists all non-coding RNA with differential expression by T treatment with adjusted p-value <0.1. Complete list of all ncRNAs is included in Supplementary Table S5.

Correlation between ncRNA and coding RNA: Differential gene correlation analyses revealed that the expression of several coding RNA was significantly correlated with that of ncRNA. In ECAT, expression of *miR-3959* was correlated with that of *HOXB6*, while *miR-381* correlated with *TNRC6C* expression and *miR-485* with *LMOD1* expression (Fig. 5 -left panel). In VAT, *miR-3955* expression correlated with *ITGB2* expression while snoRNA of the SNORA25 family - *LOC114110211* expression correlated with *TRDN and UGGT1* and *LOC114114240* expression correlated with that of *LMTK3* (Fig. 5- right panel).

3.3. BPA treatment effect

Analyses of ncRNA classes in VAT found one lncRNA (*LOC105602517*) to be marginally increased (adjusted p-value <0.1) and two snRNAs (*LOC114117093* and *LOC114117060*) to be significantly increased in the BPA-treated group (Fig. 6 – top panel). Multivariate analysis by PCA and OPLS-DA of miRNA expression showed significant separation between control and BPA-treated groups in VAT (Fig. 6 – bottom panel). Other ncRNA classes in VAT and all ncRNAs in SAT did not meet significance criteria (Supplementary Figs. S2 and S3). Full results for all ncRNA are included in Supplementary Table S6. The ncRNA that had significant (adjusted p-value <0.05) or marginal (adjusted p-value<0.1) changes in expression were not correlated with coding RNA expression levels. Log-fold change effect estimates between prenatal T treatment and BPA treatment were not strongly correlated (Supplementary Fig. S4).

3.4. Model effect

Comparison of ncRNA expression profiles in the SAT and VAT depots of controls from the two cohorts (artificial follicular phase [T-treatment cohort] and natural follicular phase [BPA-treatment cohort]) identified only one significant miRNA – *miR-374b* in the VAT (Supplementary Fig. S5) and none in the SAT. Complete list of all ncRNA are listed in Supplementary Table S7.

4. Discussion

In parallel with our earlier findings of adipose depot-specific mRNA changes in sheep exposed prenatally to T (an endogenous steroid) or BPA (an environmental steroid mimic) (Dou et al., 2020, 2021a), adipose depot-specific changes in ncRNA profiles were also evident. While specific relationships between all individual ncRNA and coding genes could not be established, owing to the underlying limitations of working with the marginally annotated sheep genome (Weikard et al., 2017), these findings point towards a possible depot-specific regulation of transcription at the epigenetic level, involving ncRNA. This is the first report of the impact of exposure to inappropriate maternal steroid milieu (T or BPA) on multiple ncRNAs namely, miRNA, lncRNA, snRNA and snoRNA at the level of various adipose tissue depots. The implications of the adipose depot-specific changes in the ncRNA profile are discussed below.

4.1. Depot-specific differences in ncRNA expression among control animals

4.1.1. Controls in the prenatal T-model

Expression profiling of ncRNA in the various adipose depots in control animals found the least differences in the VAT and the most in the ECAT depot when compared to the other depots. This parallels our previous results from the transcriptional profiling of the coding RNAs in the 4 different adipose depots from the same animals, that showed VAT had the least and ECAT had the largest number of differentially expressed coding genes relative to the other adipose tissue depots (Dou

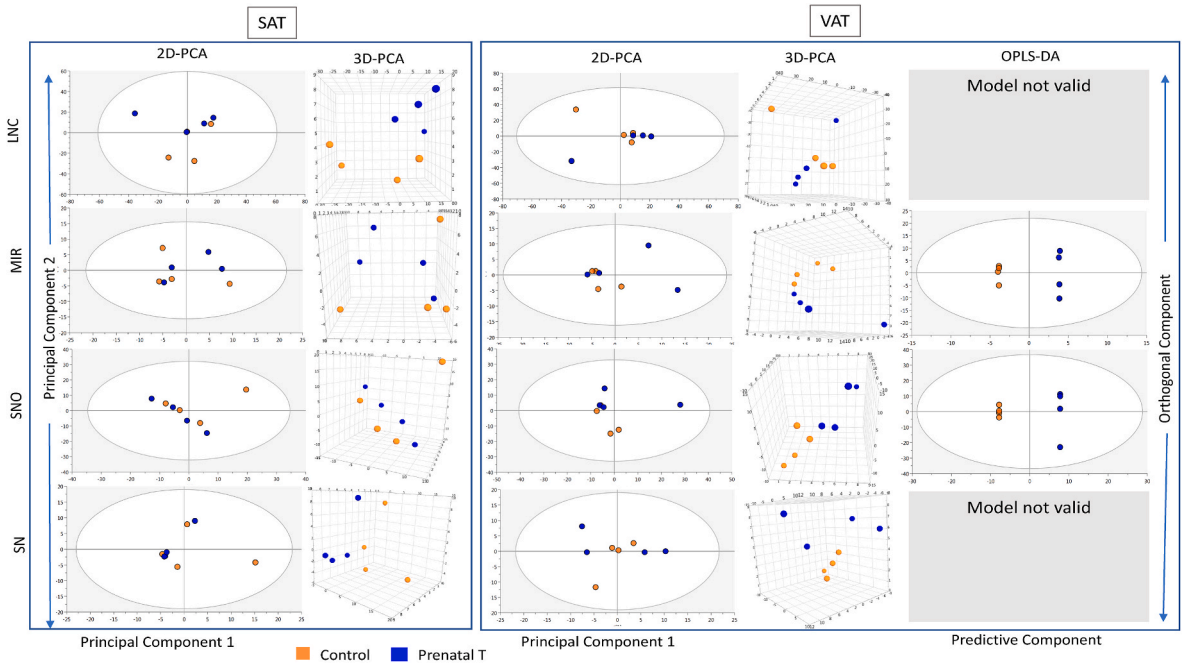

Fig. 4. Overall patterns of ncRNA expression in SAT and VAT in response to prenatal T-treatment: Principal Component Analysis (PCA) - 2-Dimensional (2D) and 3-Dimensional (3D) score plots and Orthogonal projections to latent structure discriminant analysis (OPLS-DA) score plots on lncRNA, miRNA, snoRNA, and snRNA.

Table 1
Differential expression of non-coding RNAs in ECAT, PRAT and VAT in prenatal T-treated cohort of sheep. (No differences were evident in SAT).

Gene	Control	Prenatal T	log2FC	SE	P-value	P-adj[a]
ECAT miRNA						
miR-99A	49268.53	101039	0.91	0.3	2.97E-04	0.02
miR-150	4801.36	2435.59	-0.83	0.3	7.32E-04	0.02
miR-485	236.96	107.25	-0.96	0.35	5.66E-04	0.02
miR-10B	509.3	1272.02	1.05	0.46	1.54E-03	0.03
miR-143	13823.15	35820.35	1.11	0.46	1.13E-03	0.03
miR-3959	34.56	107.86	1.28	0.58	1.40E-03	0.03
miR-433	160.52	78.3	-0.83	0.36	1.87E-03	0.03
miR-199A	8914.48	16225.99	0.72	0.3	2.53E-03	0.03
miR-218A	106.18	247.73	0.95	0.45	2.53E-03	0.03
miR-543	244.51	124.22	-0.78	0.35	2.77E-03	0.03
miR-148A	2479.8	4846.34	0.74	0.39	7.23E-03	0.06
miR-LET7B	129311.9	67193	-0.69	0.39	8.60E-03	0.07
miR-152	436.75	836.57	0.67	0.4	1.18E-02	0.08
miR-29B-1	34.52	67.9	0.7	0.44	1.22E-02	0.08
miR-29B-2	34.52	67.9	0.7	0.44	1.22E-02	0.08
miR-LET7F	11419.44	23705.63	0.72	0.48	1.40E-02	0.08
miR-381	2.29	8.93	0.68	1.34	1.56E-02	0.09
miR-10A	245.72	459.34	0.61	0.41	1.86E-02	0.09
PRAT miRNA						
miR-133	1039.3	209.15	-1.98	0.64	7.95E-05	0.008
VAT miRNA						
miR-3955	2.19	13.15	2.17	0.85	4.58E-04	0.047
VAT snoRNA						
LOC114117654	0.18	13.2	4.43	1.47	1.02E-04	0.013
LOC114110216	0.18	13.26	4.43	1.5	1.27E-04	0.013
LOC114110211	2.1	24.4	3	1.02	9.88E-05	0.013
LOC114112592	0.18	13.26	4.43	1.5	1.27E-04	0.013
LOC114114240	1.72	18.63	2.71	1.22	6.62E-04	0.05

[a] ncRNAs with adjusted P values < 0.1 are represented in the table.

et al., 2021a). The ECAT transcriptome is known to have a unique profile compared to other adipose depots (McAninch et al., 2015; Schleinitz et al., 2020) and consistent with this, it also has a unique ncRNA profile. This may relate to the fact that ECAT is physiologically (Bambace et al., 2011) and functionally divergent from the other fat depots, serving as energy source of the myocardium with cardioprotective properties (Villasante Fricke and Iacobellis, 2019). ECAT also had the largest number of snoRNA that were differentially expressed compared to the other adipose depots, although their specific function in ECAT is unknown. Functionally, snoRNA are well-conserved, housekeeping molecules that maintain ribosomal maturation and translation (Wajahat et al., 2021) and several snoRNAs play a role in metabolism in adipose tissue (Amri and Scheideler, 2017; Schaffer, 2020). ECAT and SAT had the greatest number of differentially expressed miRNA compared to the other adipose depots. There were 10 miRNA – *miR- 103, miR-127, miR-133, miR- 152, miR- 329A, miR- 329B, miR- 369, miR- 370, miR-411A, miR-487B* that were differentially expressed in both ECAT and SAT depots. *miR-103*, a key player in white adipose tissue differentiation and function (Xie et al., 2009), and *miR-152*, positively correlated with adipogenesis (Fan et al., 2019), were over-expressed in SAT and downregulated in ECAT compared to the other adipose depots. In contrast, *miR-127*, which attenuates adipogenesis (Gao et al., 2019) and *miR-133*, which regulates adipocyte browning (Liu et al., 2013) were over-expressed in ECAT and downregulated in SAT. The other identified miRNAs had no documented functional relationship with adipocytes. The change in direction of expression of these key ncRNA involved in adipogenesis and adipose browning between the ECAT and SAT corroborate the underlying functional differences between these two depots. While SAT is predominantly composed of white adipocytes, ECAT has a higher proportion of brown adipocytes. snRNA, which plays an important role in intron splicing and other mRNA pre-processing (Hari et al., 2019), did not differ between the 4 depots, suggestive of a similar functional role in all adipose tissue depots. In terms of lncRNA, PRAT showed the most changes relative to the other adipose depots, although the functions of these in PRAT remains to be identified. In general, lncRNA appear to play a role in adipogenesis (Squillaro et al., 2020) and has been implicated in insulin resistance (Tello-Flores et al., 2021) and type 2 diabetes (Guo et al., 2019).

4.1.2. Controls in the prenatal BPA model

Comparison of ncRNA profiles in the SAT and VAT revealed differences in expression of all the four types of ncRNA. Amongst the miRNAs that were downregulated in VAT compared to SAT, *miR-10B* (Li et al., 2018a) and *miR-26B* (Acharya et al., 2019) suppress adipogenic differentiation and *miR-152* is positively correlated with adipogenesis (Fan et al., 2019). Upregulated miRNAs in VAT include *miR-432* known to inhibit adipose differentiation (Jin et al., 2022), *miR*-127 that attenuates adipogenesis (Gao et al., 2019), and *miRs-200b* (Jin et al., 2021) and *-218A* (Shan et al., 2022) that facilitate the proliferation but suppress the differentiation of preadipocytes. In contrast, miRNA upregulated in SAT include *miR-148A* (Duan et al., 2021) and *miR-21* (Kim et al., 2009) that promote adipogenic differentiation, *miR-17* -a part of a cluster that accelerates adipocyte differentiation (Huang et al., 2015), *miR-221* (Ahonen et al., 2021), *miR-23A* (Shen et al., 2016), and *miR-27A* (Kim et al., 2010) that reduce adipocyte lipid storage and differentiation, and *miR-29A* that plays a pivotal role in glucose transport and lipid metabolism (Massart et al., 2017). While both represent white adipose depots, these differences in expression of various miRNAs in VAT and SAT likely reflect their functional differences. This is consistent with the key differences that prevail between VAT and SAT in their gene expression profiles (Dou et al., 2020), lipid metabolism, adipokine secretion (Malodobra-Mazur et al., 2020) and insulin sensitivity (Liu et al., 2018). The functional role of the lncRNA, snoRNA and snRNA identified to be differentially expressed between the two depots is unknown.

4.2. Comparison of the impact of T (an endogenous steroid) and BPA (an environmental steroid mimic) on ncRNA profile in adipose tissue depots

The functional similarities between the prenatal T and BPA models led us to suspect possible overlap in ncRNA profiling in the VAT and SAT depots of both the models, with expansion to ECAT and PRAT in the prenatal T model.

4.2.1. Prenatal T model

The depot-specific changes in expression of several ncRNA parallel their functional differences. With regard to changes in ncRNA

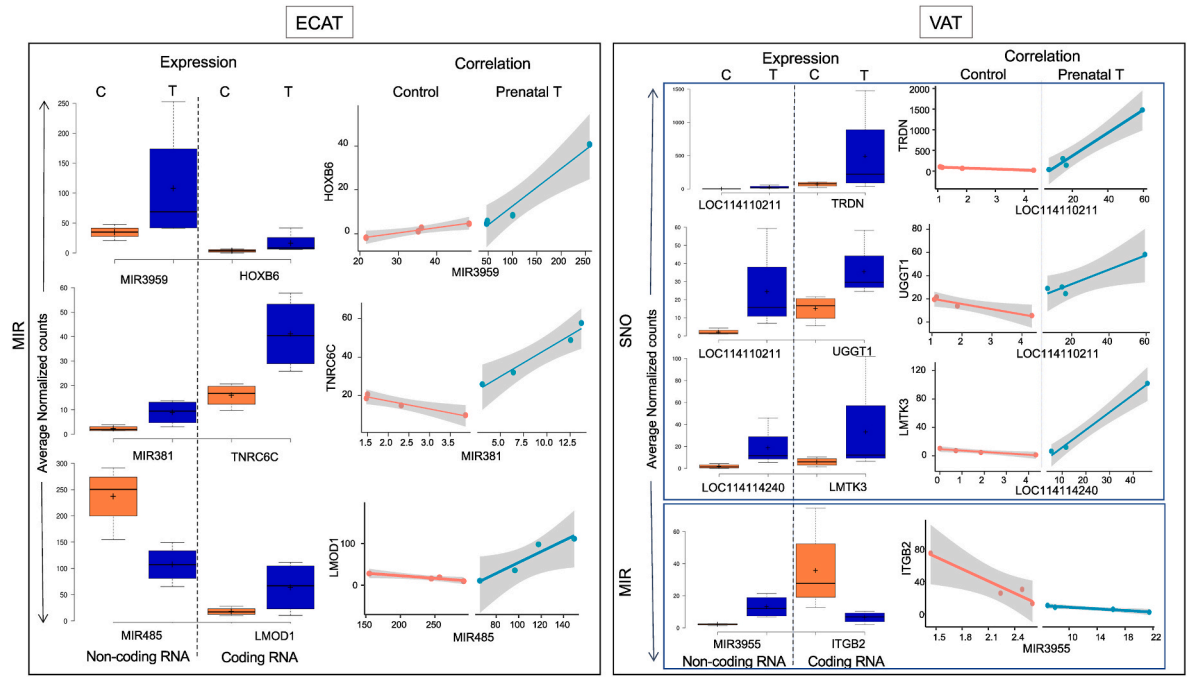

Fig. 5. Correlation between coding and ncRNA in response to prenatal T-treatment in ECAT and VAT: Left panel shows box plots representing expression level of ncRNA and mRNA and right panel shows line plots representing correlation of expression between ncRNA and mRNA in ECAT and VAT. Correlation between ncRNA-mRNA, for each pair is represented in orange line for Control animals and as a blue line for prenatal T-treated animals.

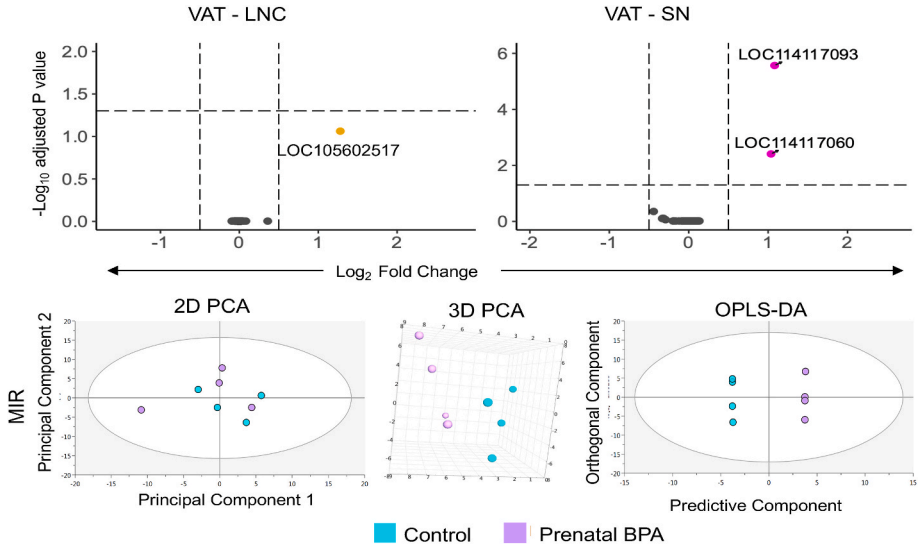

Fig. 6. ncRNA expression in VAT in response to prenatal BPA treatment: Top panel- Volcano plot representation of differential expression of lncRNA in VAT and snRNA in VAT. ncRNA are plotted by log2 fold change on the x-axis and –log10 *P* adjusted values on the y-axis. Pink points represent the genes that have an absolute log2 fold change greater than 0.5 and *P* adjusted values less than 0.05. Grey dots represent genes that did not meet *P*-adjusted cutoff of less than 0.05 and absolute $\log_2$ fold change greater than 0.5 and yellow dots represent genes that met the absolute $\log_2$ fold change greater than 0.5 but did not meet the *P*-adjusted cutoff of less than 0.05. Bottom panel - Principal Component Analysis (PCA) - 2D and 3D score plots and Orthogonal projections to latent structure discriminant analysis (OPLS-DA) score plots on miRNA.

expression in the ECAT, many of the dysregulated miRNAs are involved in glucose metabolism and insulin resistance, which are contributors to cardiometabolic disorders (Iacobellis, 2022). Phenotypically, prenatal T-treated females exhibit hypertension (King et al., 2007) and left ventricular hypertrophy along with an increased expression of genes involved in insulin signaling in left ventricular tissue (Vyas et al., 2016). Several miRNAs altered by prenatal T excess have been associated with cardiac hypertrophy. For instance, overexpression of *miR-99A*, which is regulated by insulin (Li et al., 2013) and plays an important role in glucose metabolism (Kim and Zhang, 2019; Ye et al., 2022), is known to attenuate cardiac hypertrophy (Li et al., 2016, 2016v; van Rooij et al., 2006). Similarly, *miR-143* over-expressed in ECAT, is involved in insulin resistance in brown adipose tissue (Ono, 2011) and adipocyte differentiation (Esau et al., 2004) and is also over-expressed in obesity-induced cardiac hypertrophy in female mice (de Oliveira Silva et al., 2022). Another upregulated miRNA, *miR-10B*, is upregulated in ventricular tissue of hypertrophic cardiomyopathy patients (Li et al., 2018b). Other members of the *miR-10b* family are differentially expressed in the ECAT of coronary artery disease patients (Flinn et al., 2022). In addition, upregulation of this mRNA is shown to be associated with obesity associated dyslipidemia and adipokine expression (Gu et al., 2016) and reduction of thermogenic brown adipocyte differentiation in humans (Gao et al., 2018), features that promote insulin resistance. Among the downregulated miRNAs in ECAT, *miR-150* is associated with cardiac hypertrophy (Liu et al., 2015). The downregulated *miR-485,* also observed in the ECAT of patients with coronary atherosclerosis (Jinxing et al., 2022) is known to suppress hypertrophy in cardiomyocytes (Zhao et al., 2017). In line with the transcriptome profile of ECAT in prenatal

T-treated sheep, which showed dysregulation of genes involved in cardiomyocyte function, the miRNA dysregulated in ECAT like *miR-433* (Tao et al., 2016), *miR-199* (Ouyang and Wei, 2021) and *miR-143* (Ogawa et al., 2020) also play pivotal roles in cardiomyocyte function. Thus, the miRNA profile in ECAT is consistent with the observed phenotypic changes involving hypertrophy (Vyas et al., 2016). None of the other ncRNAs examined including lncRNA, snRNA, and snoRNA were impacted by prenatal T excess in the ECAT.

In PRAT, the decreased expression of *miR-133*, a well-known brown adipogenesis inhibitor (Liu et al., 2013; Gharanei et al., 2020), is consistent with the increased expression of the thermogenic gene *UCP1* indicative of increased browning (Puttabyatappa et al., 2020). The functional role of the *miR-3955* and the 4 snoRNAs that are overexpressed in VAT tissue of prenatal T-treatment is unknown. Interestingly, SAT which showed an upregulation of chromatin modification pathways in the transcriptome analysis (Dou et al., 2021a) did not have any significant differentially expressed ncRNA in response to prenatal T-treatment. Prenatal T-treatment did not result in a difference in the expression of any snRNA or lncRNA in any of the adipose depots, indicating the possible involvement of other epigenetic mechanisms of regulation like DNA methylation or histone modification.

4.2.2. Prenatal BPA model

Although transcriptome analyses of adipose depots in response to prenatal BPA-treatment had identified upregulation of chromatin modeling pathways and mRNA processing pathways in VAT and RNA splicing pathways in SAT (Dou et al., 2020), similar to findings in the prenatal T model, BPA treatment had no effect on any of the ncRNA in SAT depot. In contrast, the VAT showed increased expression of one lncRNA and two snRNA (no impact on miRNA), the roles of which remain to be functionally characterized. ECAT and PRAT were not studied in this model.

Comparing the impact of prenatal impact of T and BPA in VAT and SAT depots (only depots studied in both models), there was no impact of either treatment on any of the ncRNA studied in the SAT. In contrast, in the VAT, prenatal T resulted in overexpression of *miR-3955* and 4 snoRNAs while prenatal BPA exposure resulted in the overexpression of one lncRNA and two snRNAs with no overlap between the two models, indicative of a mutually exclusive outcome in the ncRNA profile. While prenatal T-treatment had no effect on snRNA and lncRNA, prenatal BPA-treatment had no effect on miRNA and snoRNA expression, suggestive of mediation via different steroid receptor systems and involvement of other epigenetic modulators.

4.3. Correlation between coding RNA and ncRNA

Non-coding RNAs play an important role in regulating the coding RNA expression by several mechanisms (Statello et al., 2021) and correlation of miRNA and mRNA expression has helped in comprehending the biological mechanisms and regulatory processes involved in metabolic disorders (Kirby et al., 2016; Mencucci et al., 2022).

4.3.1. Prenatal T model

In ECAT, the changes in expression of three miRNAs were correlated with coding RNA expression. The expression of miR-3959, which has an important role in energy metabolism (Shi et al., 2020) was correlated with that of *HOXB6,* identified as a pre-adipocyte precursor gene (Fainberg et al., 2018). *miR-381* expression which has a role in brown adipocyte differentiation (Keller et al., 2011) correlated with expression of *TNRC6C* which plays a role in RNA-mediated gene silencing by miRNA (Lazzaretti et al., 2009) and circular RNA degradation (Jia et al., 2019). *miR*-485 has a role in adipocyte differentiation (Guo and Cao, 2019) and its expression correlated with that of *LMOD1,* which is involved in smooth muscle differentiation and associated with coronary artery disease (Nanda and Miano, 2012; Nanda et al., 2018). In VAT, the expression of one miRNA and two snoRNAs correlated with the expression of coding genes. *miR-3955* expression correlated with that of *ITGB2*, known to be upregulated in obesity (Nair et al., 2005), type 2 diabetes (Carruthers et al., 2021) and insulin resistance (Soronen et al., 2012). *ITGB2* encodes an integrin beta chain that is a part of integrin heterodimers that regulate white adipose tissue insulin sensitivity and brown fat thermogenesis (Ruiz-Ojeda et al., 2021). The expression of the snoRNA *LOC114110211* correlated with *TRDN and UGGT1* gene expression. While *TRDN* is upregulated in obesity (Dong et al., 2021) and diabetes (Mussa et al., 2022), *UGGT1* is a glycoprotein glucosyltransferase whose expression is associated with obesity in humans (Zhang et al., 2022) and increased in obese - type 2 diabetes rat model (Kuribara et al., 2020), indicating a potential role for *LOC114110211* in regulating metabolism. *LOC114114240* expression correlated with the expression of a tyrosine kinase *LMTK3,* which phosphorylates the estrogen receptor (Giamas et al., 2011), shown to regulate insulin sensitivity (Muraki et al., 2006), beiging of adipocytes (Santos et al., 2018) and has a central role in energy homeostasis (Barros and Gustafsson, 2011).

4.3.2. Prenatal BPA model

There were no significant correlations between the ncRNA and any of the significant differentially expressed coding RNA identified from the earlier total transcriptome analysis. This may be because of the limited number of ncRNA that were identified as differentially expressed in this model.

4.4. Impact of prenatal T vs. BPA on ncRNA profiles-differences

There was very little overlap relative to the impact on prenatal T vs. BPA on VAT and SAT ncRNA expression pattern, although these animals manifested similar metabolic outcomes in terms of their insulin resistance albeit, of different severity. These differences in ncRNA profile may relate to the modes of action of T and BPA. The androgen, T, signals through androgen receptor but has the potential to be aromatized and activate estrogen receptor. Indeed, prenatal T-treatment increases estradiol levels in the female fetuses (Veiga-Lopez et al., 2011). On the other hand, BPA is a weak estrogen and shown to be an androgen antagonist (Wang et al., 2017). Both models manifest hyperinsulinemia that have the potential to work through insulin receptor (Nada et al., 2010). Alternatively, the T model used an artificial follicular phase model where animals are ovariectomized and replaced with steroids mimicking that seen in the ovary intact model. Another difference was that the T model received twice weekly intramuscular injections of T and no vehicle treatment for controls, while BPA model received daily subcutaneous injections of BPA with controls receiving daily vehicle treatment. However, comparison of ncRNA profile to address the underlying differences in the controls of the two cohorts found no difference in the SAT and marginal difference in VAT (1 miRNA) indicating the two cohorts (ovary intact and artificial follicular phase models) are comparable and vehicle treatment differences does not exist. Our earlier study has also indicated the absence of phenotypic changes in response to vehicle treatment in sheep (Veiga-Lopez et al., 2008).

4.5. Strengths and limitations

Adipose depots are recently gaining significance for their pivotal role in regulating energy metabolism and insulin resistance (Bodis and Roden, 2018; Fernandez-Verdejo et al., 2019). In addition to the established roles of VAT and SAT, ECAT and PRAT have emerged as important risk factors for cardiometabolic disorders (Huang et al., 2020; Le Jemtel et al., 2019). While VAT and SAT have been extensively studied, molecular studies on ECAT and PRAT from humans are scarce due to the limited availability of these tissues for molecular analyses, that has resulted in a limited understanding of the underlying biology of these adipose depots. There is a gap in research on studies comparing the different adipose depots apart from a few in mouse models (Chen et al.,

2022; Yamamoto et al., 2010) and a meta-analysis (Lenz et al., 2020). Our study gives a comprehensive understanding of the ncRNA expression profile in all the four adipose depots in response to prenatal T treatment and in VAT and SAT on prenatal BPA treatment. The observed depot-specific ncRNA changes reiterate that molecular and functional differences exist between the various adipose depots. Although both models manifest an insulin resistance phenotype, the adipocyte impact from ncRNA in VAT and SAT is mutually exclusive. Another strength is correlating the ncRNA expression changes with the coding RNA changes in the same samples to delineate their potential contribution to regulation of coding genes (Dou et al., 2020, 2021a). An important advantage of this study is the use of a large precocial animal model that has a translational relevance to humans (Gonzalez-Bulnes and Chavatte-Palmer, 2017), owing to similarities in their developmental trajectories.

A major limitation of this study is the non-availability of comprehensive annotation details for sequences from sheep and lack of sufficient functional characterization. The miRbase, which is a comprehensive database of miRNA including precursor and mature mRNA, includes 4571 miRNAs for humans, 3212 miRNAs for mouse (Kozomara et al., 2019) but only 259 for sheep. The same is true for the other classes of ncRNA. This has been a major deterrent to identify more differential ncRNA and make functional correlations of the observed ncRNA differences in our study, as some of the differential ncRNA that we identified were uncharacterized. To facilitate future sheep annotation studies, we have made our raw sequencing data public. The use of a small number of samples for the analyses may have also limited the identification of more differentially expressed ncRNAs. Paradoxically, a smaller number of snoRNA that were identified in the earlier total transcriptome analysis of the coding genes in the prenatal -T and -BPA cohorts (Dou et al., 2020, 2021a) were not identified in the current study. This may be due to the difference in the RNA extraction and sequencing analysis procedures for the two analyses.

4.6. Translational significance

Metabolic disorders like diabetes (Cho et al., 2018), hypertension (Mills et al., 2020), and cardiovascular disorders (Thomas et al., 2018) have been on the rise in low- and middle-income countries. Different adipose depots have specific roles to play in the development of metabolic disorders (Bjorndal et al., 2011; Chait and den Hartigh, 2020) and adipose depot measures have been identified as early risk factors for cardiovascular disorders (Eisenberg et al., 2020; Lopez-Bermejo et al., 2019), hypertension (Sasaki et al., 2022), and diabetes (Lee et al., 2019). In fact, transplantation of PRAT from healthy donors has been proposed as a therapeutic option to treat metabolic disease (AlZaim et al., 2020). While structural, functional and molecular differences between VAT and SAT (Ibrahim, 2010) have been identified in humans and mouse models (Komolka et al., 2014), similar comparisons in other depots including ECAT and PRAT are minimal in humans and are restricted to indirect measurements of fat depots with imaging and spectroscopy (Komolka et al., 2014). In this context, our study that document differences in the ncRNA profile across four different depots that parallel the direction of changes in coding RNA profile in a sheep model of PCOS phenotype, is of relevance to organ-specific regulation exerted by specific adipose depots. The literature available on VAT depots in humans is primarily from obese individuals undergoing bariatric surgery (Van Harmelen et al., 2004) or cardiac or abdominal surgery (Schoof et al., 2004). In contrast, our data from animals raised on maintenance diet to avoid confounding raising from obesity (Veiga-Lopez et al., 2013a) may be of a broader applicability.

5. Conclusions

This study illustrates that prenatal T and BPA treatments program adipose depot-specific ncRNA changes in sheep. We identified changes in ncRNA that link to the previously reported transcriptional changes in these models. This also suggests prenatal exposure to the endogenous steroid, testosterone and environmental steroid mimic, bisphenol A could have different epigenetic mechanisms of action on the different adipose tissue depots. Overall, our study presents a comprehensive overview of the ncRNA landscape of the different adipose depots.

CRediT authorship contribution statement

John Dou: Formal analysis, Visualization, Writing – original draft. **Soundara Viveka Thangaraj:** Formal analysis, Visualization, Writing – original draft. **Muraly Puttabyatappa:** Investigation, Writing – review & editing. **Venkateswaran Ramamoorthi Elangovan:** Formal analysis, Writing – review & editing. **Kelly Bakulski:** Writing – review & editing, Resources, Supervision. **Vasantha Padmanabhan:** Conceptualization, Methodology, Supervision, Writing – original draft, Writing – review & editing, Resources, Project administration, Funding acquisition.

Declaration of competing interest

Authors have nothing to disclose.

Data availability

Link to data/code in the manuscript has been shared.

Acknowledgement

We thank Mr. Douglas Doop for help with breeding, lambing and maintenance of sheep used in the study, Ms. Carol Herkimer, Dr. Almudena Veiga-Lopez, Mr. Evan Beckett and the several undergraduate students from the University of Michigan Undergraduate Research Opportunity Program for assistance during animal experimentation and procurement of the various adipose tissue depots.

Appendix A. Supplementary data

Supplementary data to this article can be found online at https://doi.org/10.1016/j.mce.2023.111868.

References

Abruzzese, G.A., et al., 2018. Developmental programming of the female neuroendocrine system by steroids. J. Neuroendocrinol. 30 (10), e12632.
Acharya, A., et al., 2019. miR-26 suppresses adipocyte progenitor differentiation and fat production by targeting Fbxl19. Genes Dev. 33 (19–20), 1367–1380.
Agbu, P., Carthew, R.W., 2021. MicroRNA-mediated regulation of glucose and lipid metabolism. Nat. Rev. Mol. Cell Biol. 22 (6), 425–438.
Ahonen, M.A., et al., 2021. Human adipocyte differentiation and composition of disease-relevant lipids are regulated by miR-221-3p. Biochim. Biophys. Acta Mol. Cell Biol. Lipids 1866 (1), 158841.
AlZaim, I., et al., 2020. Adipose tissue immunomodulation: a novel therapeutic approach in cardiovascular and metabolic diseases. Front. Cardiovasc. Med. 7, 602088.
Amri, E.Z., Scheideler, M., 2017. Small non coding RNAs in adipocyte biology and obesity. Mol. Cell. Endocrinol. 456, 87–94.
Andrews, S., 2010. FastQC: A Quality Control Tool for High Throughput Sequence Data.
Arner, P., Ryden, M., 2022. Human white adipose tissue: a highly dynamic metabolic organ. J. Intern. Med. 291 (5), 611–621.
Bambace, C., et al., 2011. Adiponectin gene expression and adipocyte diameter: a comparison between epicardial and subcutaneous adipose tissue in men. Cardiovasc. Pathol. 20 (5), e153–e156.
Barouki, R., et al., 2012. Developmental origins of non-communicable disease: implications for research and public health. Environ. Health 11, 42.
Barros, R.P., Gustafsson, J.A., 2011. Estrogen receptors and the metabolic network. Cell Metabol. 14 (3), 289–299.
Bjorndal, B., et al., 2011. Different adipose depots: their role in the development of metabolic syndrome and mitochondrial response to hypolipidemic agents. J. Obes. 2011, 490650.
Blighe, K., Rana, S., Lewis, M., 2021. EnhancedVolcano: Publication-Ready Volcano Plots with Enhanced Colouring and Labeling.
Bodis, K., Roden, M., 2018. Energy metabolism of white adipose tissue and insulin resistance in humans. Eur. J. Clin. Invest. 48 (11), e13017.

Bratkovič, T., Božič, J., Rogelj, B., 2020. Functional diversity of small nucleolar RNAs. Nucleic Acids Res. 48 (4), 1627–1651.
Cardoso, R.C., Padmanabhan, V., 2019. Prenatal steroids and metabolic dysfunction: lessons from sheep. Annu. Rev. Anim. Biosci. 7, 337–360.
Cardoso, R.C., et al., 2016. Developmental programming: impact of gestational steroid and metabolic milieus on adiposity and insulin sensitivity in prenatal testosterone-treated female sheep. Endocrinology 157 (2), 522–535.
Carruthers, N.J., et al., 2021. The human type 2 diabetes-specific visceral adipose tissue proteome and transcriptome in obesity. Sci. Rep. 11 (1), 17394.
Chait, A., den Hartigh, L.J., 2020. Adipose tissue distribution, inflammation and its metabolic consequences, including diabetes and cardiovascular disease. Front. Cardiovasc. Med. 7, 22.
Chao, Y., et al., 2021. Regulatory roles and mechanisms of alternative RNA splicing in adipogenesis and human metabolic health. Cell Biosci. 11 (1), 66.
Chao, Y., et al., 2022. Dysregulated adipose tissue expansion and impaired adipogenesis in Prader-Willi syndrome children before obesity-onset. Metabolism 136, 155295.
Chen, M., et al., 2022. Omics approach to reveal the effects of obesity on the protein profiles of the exosomes derived from different adipose depots. Cell. Mol. Life Sci. 79 (11), 570.
Cho, N.H., et al., 2018. IDF Diabetes Atlas: global estimates of diabetes prevalence for 2017 and projections for 2045. Diabetes Res. Clin. Pract. 138, 271–281.
de Oliveira Silva, T., et al., 2022. The miRNA-143-3p-Sox6-Myh7 pathway is altered in obesogenic diet-induced cardiac hypertrophy. Exp. Physiol. 107 (8), 892–905.
Dobin, A., et al., 2013. STAR: ultrafast universal RNA-seq aligner. Bioinformatics 29 (1), 15–21.
Dong, Z., et al., 2021. Identification of core gene in obese type 2 diabetes patients using bioinformatics analysis. Adipocyte 10 (1), 310–321.
Dou, J.F., et al., 2020. Developmental programming: transcriptional regulation of visceral and subcutaneous adipose by prenatal bisphenol-A in female sheep. Chemosphere 255, 127000.
Dou, J., et al., 2021a. Developmental programming: adipose depot-specific transcriptional regulation by prenatal testosterone excess in a sheep model of PCOS. Mol. Cell. Endocrinol. 523, 111137.
Dou, J., et al., 2021b. Developmental programming: adipose depot-specific transcriptional regulation by prenatal testosterone excess in a sheep model of PCOS. Mol. Cell. Endocrinol. 523, 111137.
Duan, D.Y., et al., 2021. Adipocyte-secreted microvesicle-derived miR-148a regulates adipogenic and osteogenic differentiation by targeting Wnt5a/Ror2 pathway. Life Sci. 278, 119548.
Eisenberg, E., et al., 2020. Deep learning-based quantification of epicardial adipose tissue volume and attenuation predicts major adverse cardiovascular events in asymptomatic subjects. Circ. Cardiovasc. Imag. 13 (2), e009829.
Esau, C., et al., 2004. MicroRNA-143 regulates adipocyte differentiation. J. Biol. Chem. 279 (50), 52361–52365.
Ewels, P., et al., 2016. MultiQC: summarize analysis results for multiple tools and samples in a single report. Bioinformatics 32 (19), 3047–3048.
Fainberg, H.P., et al., 2018. Transcriptional analysis of adipose tissue during development reveals depot-specific responsiveness to maternal dietary supplementation. Sci. Rep. 8 (1), 9628.
Fan, Y., et al., 2019. Mir-152 regulates 3T3-L1 preadipocyte proliferation and differentiation. Molecules 24 (18).
Fernandez-Verdejo, R., et al., 2019. Contribution of brown adipose tissue to human energy metabolism. Mol. Aspect. Med. 68, 82–89.
Ferreira, S.R., et al., 2021. Prenatal testosterone exposure induces insulin resistance, uterine oxidative stress and pro-inflammatory status in rats. Mol. Cell. Endocrinol. 519, 111045.
Flinn, B., et al., 2022. Profiling of non-coding regulators and their targets in epicardial fat from patients with coronary artery disease. Int. J. Mol. Sci. 23 (10).
Gao, Y., et al., 2018. miR-199a-3p regulates brown adipocyte differentiation through mTOR signaling pathway. Mol. Cell. Endocrinol. 476, 155–164.
Gao, Y., et al., 2019. MiR-127 attenuates adipogenesis by targeting MAPK4 and HOXC6 in porcine adipocytes. J. Cell. Physiol. 234 (12), 21838–21850.
Gerona, R.R., et al., 2013. Bisphenol-A (BPA), BPA glucuronide, and BPA sulfate in midgestation umbilical cord serum in a northern and central California population. Environ. Sci. Technol. 47 (21), 12477–12485.
Gharanei, S., et al., 2020. Regulatory microRNAs in Brown, brite and white adipose tissue. Cells 9 (11).
Giamas, G., et al., 2011. Kinome screening for regulators of the estrogen receptor identifies LMTK3 as a new therapeutic target in breast cancer. Nat. Med. 17 (6), 715–719.
Gonzalez-Bulnes, A., Chavatte-Palmer, P., 2017. Contribution of large animals to translational research on prenatal programming of obesity and associated diseases. Curr. Pharmaceut. Biotechnol. 18 (7), 541–551.
Goodman, R.L., et al., 1981. Importance of variations in behavioural and feedback actions of oestradiol to the control of seasonal breeding in the Ewe. J. Endocrinol. 89 (2), 229–240.
Gu, N., et al., 2016. Expression of miR-199a-3p in human adipocytes is regulated by free fatty acids and adipokines. Mol. Med. Rep. 14 (2), 1180–1186.
Guo, Z., Cao, Y., 2019. An lncRNAmiRNAmRNA ceRNA network for adipocyte differentiation from human adiposederived stem cells. Mol. Med. Rep. 19 (5), 4271–4287.
Guo, J., Liu, Z., Gong, R., 2019. Long noncoding RNA: an emerging player in diabetes and diabetic kidney disease. Clin. Sci. (Lond.) 133 (12), 1321–1339.
Hari, R., Parthasarathy, S., 2019. Prediction of coding and non-coding RNA. In: Ranganathan, S., et al. (Eds.), Encyclopedia of Bioinformatics and Computational Biology. Academic Press, Oxford, pp. 230–240.
Hartley, S.W., Mullikin, J.C., 2015. QoRTs: a comprehensive toolset for quality control and data processing of RNA-Seq experiments. BMC Bioinf. 16, 224.
Huang, H.Y., et al., 2015. Integrated analysis of microRNA and mRNA expression profiles in abdominal adipose tissues in chickens. Sci. Rep. 5, 16132.
Huang, Q., Liu, Y., Dong, S., 2018. Emerging roles of long non-coding RNAs in the toxicology of environmental chemicals. J. Appl. Toxicol. 38 (7), 934–943.
Huang, N., et al., 2020. Novel insight into perirenal adipose tissue: a neglected adipose depot linking cardiovascular and chronic kidney disease. World J. Diabetes 11 (4), 115–125.
Iacobellis, G., 2022. Epicardial adipose tissue in contemporary cardiology. Nat. Rev. Cardiol. 19 (9), 593–606.
Iacobellis, G., Leonetti, F., 2005. Epicardial adipose tissue and insulin resistance in obese subjects. J. Clin. Endocrinol. Metab. 90 (11), 6300–6302.
Ibrahim, M.M., 2010. Subcutaneous and visceral adipose tissue: structural and functional differences. Obes. Rev. 11 (1), 11–18.
Jia, R., et al., 2019. Defining an evolutionarily conserved role of GW182 in circular RNA degradation. Cell Discov. 5, 45.
Jin, X., et al., 2021. MicroRNA-200b regulates the proliferation and differentiation of ovine preadipocytes by targeting p27 and KLF9. Animals (Basel) 11 (8).
Jin, M., et al., 2022. Oar-miR-432 regulates fat differentiation and promotes the expression of BMP2 in ovine preadipocytes. Front. Genet. 13, 844747.
Jinxing, L., et al., 2022. MicroRNA expression profiles of epicardial adipose tissue-derived exosomes in patients with coronary atherosclerosis. Rev. Cardiovasc. Med. 23 (6), 206.
Keller, P., et al., 2011. Gene-chip studies of adipogenesis-regulated microRNAs in mouse primary adipocytes and human obesity. BMC Endocr. Disord. 11, 7.
Kim, M., Zhang, X., 2019. The profiling and role of miRNAs in diabetes mellitus. J. Diabetes Clin. Res. 1 (1), 5–23.
Kim, Y.J., et al., 2009. MiR-21 regulates adipogenic differentiation through the modulation of TGF-beta signaling in mesenchymal stem cells derived from human adipose tissue. Stem Cell. 27 (12), 3093–3102.
Kim, S.Y., et al., 2010. miR-27a is a negative regulator of adipocyte differentiation via suppressing PPARgamma expression. Biochem. Biophys. Res. Commun. 392 (3), 323–328.
Kim, J.I., et al., 2015. Lipid-overloaded enlarged adipocytes provoke insulin resistance independent of inflammation. Mol. Cell Biol. 35 (10), 1686–1699.
King, A.J., et al., 2007. Hypertension caused by prenatal testosterone excess in female sheep. Am. J. Physiol. Endocrinol. Metab. 292 (6), E1837–E1841.
Kirby, T.J., et al., 2016. Integrative mRNA-microRNA analyses reveal novel interactions related to insulin sensitivity in human adipose tissue. Physiol. Genom. 48 (2), 145–153.
Koenen, M., et al., 2021. Obesity, adipose tissue and vascular dysfunction. Circ. Res. 128 (7), 951–968.
Komolka, K., et al., 2014. Molecular heterogeneities of adipose depots - potential effects on adipose-muscle cross-talk in humans, mice and farm animals. J. Genom. 2, 31–44.
Kozomara, A., Birgaoanu, M., Griffiths-Jones, S., 2019. miRBase: from microRNA sequences to function. Nucleic Acids Res. 47 (D1), D155–D162.
Kumar, M., et al., 2020. Environmental endocrine-disrupting chemical exposure: role in non-communicable diseases. Front. Public Health 8, 553850.
Kuribara, T., et al., 2020. Metabolic syndrome perturbs deglucosylation and reglucosylation in the glycoprotein folding cycle. FEBS Lett. 594 (11), 1759–1769.
Lazzaretti, D., Tournier, I., Izaurralde, E., 2009. The C-terminal domains of human TNRC6A, TNRC6B, and TNRC6C silence bound transcripts independently of Argonaute proteins. RNA 15 (6), 1059–1066.
Le Jemtel, T.H., et al., 2019. Epicardial adipose tissue and cardiovascular disease. Curr. Hypertens. Rep. 21 (5), 36.
Lee, M.J., Wu, Y., Fried, S.K., 2013. Adipose tissue heterogeneity: implication of depot differences in adipose tissue for obesity complications. Mol. Aspect. Med. 34 (1), 1–11.
Lee, J., et al., 2018. Bisphenol A distribution in serum, urine, placenta, breast milk, and umbilical cord serum in a birth panel of mother-neonate pairs. Sci. Total Environ. 626, 1494–1501.
Lee, M.W., Lee, M., Oh, K.J., 2019. Adipose tissue-derived signatures for obesity and type 2 diabetes: adipokines, batokines and MicroRNAs. J. Clin. Med. 8 (6).
Lenz, M., et al., 2020. Adipose tissue in health and disease through the lens of its building blocks. Sci. Rep. 10 (1), 10433.
Li, W., et al., 2013. Insulin promotes glucose consumption via regulation of miR-99a/mTOR/PKM2 pathway. PLoS One 8 (6), e64924.
Li, Q., et al., 2016. Overexpression of microRNA-99a attenuates cardiac hypertrophy. PLoS One 11 (2), e0148480.
Li, H., et al., 2018a. MiRNA-10b reciprocally stimulates osteogenesis and inhibits adipogenesis partly through the TGF-beta/SMAD2 signaling pathway. Aging Dis. 9 (6), 1058–1073.
Li, M., et al., 2018b. MiR-1-3p that correlates with left ventricular function of HCM can serve as a potential target and differentiate HCM from DCM. J. Transl. Med. 16 (1), 161.
Li, M., et al., 2019. MicroRNAs and their role in environmental chemical carcinogenesis. Environ. Geochem. Health 41 (1), 225–247.
Li, X., Peng, J., Yi, C., 2021. The epitranscriptome of small non-coding RNAs. Non-coding RNA Res. 6 (4), 167–173.
Liao, Y., Smyth, G.K., Shi, W., 2014. featureCounts: an efficient general purpose program for assigning sequence reads to genomic features. Bioinformatics 30 (7), 923–930.
Liu, W., et al., 2013. miR-133a regulates adipocyte browning in vivo. PLoS Genet. 9 (7), e1003626.
Liu, W., et al., 2015. MicroRNA-150 protects against pressure overload-induced cardiac hypertrophy. J. Cell. Biochem. 116 (10), 2166–2176.

Liu, L., et al., 2018. Visceral adipose tissue is more strongly associated with insulin resistance than subcutaneous adipose tissue in Chinese subjects with pre-diabetes. Curr. Med. Res. Opin. 34 (1), 123–129.
Liu, B.X., Sun, W., Kong, X.Q., 2019. Perirenal fat: a unique fat pad and potential target for cardiovascular disease. Angiology 70 (7), 584–593.
Lopez-Bermejo, A., et al., 2019. Perirenal and epicardial fat and their association with carotid intima-media thickness in children. Ann. Pediatr. Endocrinol. Metab. 24 (4), 220–225.
Love, M.I., Huber, W., Anders, S., 2014. Moderated estimation of fold change and dispersion for RNA-seq data with DESeq2. Genome Biol. 15 (12), 550.
Lu, C., et al., 2016. Developmental programming: prenatal testosterone excess and insulin signaling disruptions in female sheep. Biol. Reprod. 94 (5), 113.
Luo, L., Liu, M., 2016. Adipose tissue in control of metabolism. J. Endocrinol. 231 (3), R77–R99.
Luo, F., et al., 2016. The lncRNA MALAT1, acting through HIF-1alpha stabilization, enhances arsenite-induced glycolysis in human hepatic L-02 cells. Biochim. Biophys. Acta 1862 (9), 1685–1695.
Luong, Q., Huang, J., Lee, K.Y., 2019. Deciphering white adipose tissue heterogeneity. Biology 8 (2).
Maliszewska, K., Kretowski, A., 2021. Brown adipose tissue and its role in insulin and glucose homeostasis. Int. J. Mol. Sci. 22 (4).
Malodobra-Mazur, M., et al., 2020. Metabolic differences between subcutaneous and visceral adipocytes differentiated with an excess of saturated and monounsaturated fatty acids. Genes 11 (9).
Manikkam, M., et al., 2004. Fetal programming: prenatal testosterone excess leads to fetal growth retardation and postnatal catch-up growth in sheep. Endocrinology 145 (2), 790–798.
Martin, M., 2011. Cutadapt removes adapter sequences from high-throughput sequencing reads. EMBnet. J. 10–12.
Massart, J., et al., 2017. Altered miR-29 expression in type 2 diabetes influences glucose and lipid metabolism in skeletal muscle. Diabetes 66 (7), 1807–1818.
McAninch, E.A., et al., 2015. Epicardial adipose tissue has a unique transcriptome modified in severe coronary artery disease. Obesity 23 (6), 1267–1278.
McKenzie, A.T., et al., 2016. DGCA: A comprehensive R package for differential gene correlation analysis. BMC Syst. Biol. 10 (1), 106.
Mencucci, M.V., et al., 2022. Identification of novel microRNAs associated with type 2 diabetes by an integrative bioinformatic analysis. Hum. Genet. 34, 201125.
Mills, K.T., Stefanescu, A., He, J., 2020. The global epidemiology of hypertension. Nat. Rev. Nephrol. 16 (4), 223–237.
Muraki, K., Okuya, S., Tanizawa, Y., 2006. Estrogen receptor alpha regulates insulin sensitivity through IRS-1 tyrosine phosphorylation in mature 3T3-L1 adipocytes. Endocr. J. 53 (6), 841–851.
Mussa, B.M., et al., 2022. Identification of novel differentially expressed genes in type 1 diabetes mellitus complications using transcriptomic profiling of UAE patients: a multicenter study. Sci. Rep. 12 (1), 16316.
Nada, S.E., Thompson, R.C., Padmanabhan, V., 2010. Developmental programming: differential effects of prenatal testosterone excess on insulin target tissues. Endocrinology 151 (11), 5165–5173.
Nair, S., et al., 2005. Increased expression of inflammation-related genes in cultured preadipocytes/stromal vascular cells from obese compared with non-obese Pima Indians. Diabetologia 48 (9), 1784–1788.
Nanda, V., Miano, J.M., 2012. Leiomodin 1, a new serum response factor-dependent target gene expressed preferentially in differentiated smooth muscle cells. J. Biol. Chem. 287 (4), 2459–2467.
Nanda, V., et al., 2018. Functional regulatory mechanism of smooth muscle cell-restricted LMOD1 coronary artery disease locus. PLoS Genet. 14 (11), e1007755.
Ogawa, K., et al., 2020. Forced expression of miR-143 and -145 in cardiomyocytes induces cardiomyopathy with a reductive redox shift. Cell. Mol. Biol. Lett. 25, 40.
Ono, K., 2011. MicroRNA links obesity and impaired glucose metabolism. Cell Res. 21 (6), 864–866.
Ouyang, Z., Wei, K., 2021. miRNA in cardiac development and regeneration. Cell Regen. 10 (1), 14.
Padmanabhan, V., Veiga-Lopez, A., 2013. Sheep models of polycystic ovary syndrome phenotype. Mol. Cell. Endocrinol. 373 (1–2), 8–20.
Padmanabhan, V., et al., 2010. Developmental reprogramming of reproductive and metabolic dysfunction in sheep: native steroids vs. environmental steroid receptor modulators. Int. J. Androl. 33 (2), 394–404.
Patni, N., Garg, A., 2022. Lipodystrophy for the diabetologist-what to look for. Curr. Diabetes Rep. 22 (9), 461–470.
Puttabyatappa, M., Padmanabhan, V., 2017. Prenatal testosterone programming of insulin resistance in the female sheep. Adv. Exp. Med. Biol. 1043, 575–596.
Puttabyatappa, M., et al., 2017. Developmental programming: impact of gestational steroid and metabolic milieus on mediators of insulin sensitivity in prenatal testosterone-treated female sheep. Endocrinology 158 (9), 2783–2798.
Puttabyatappa, M., et al., 2018. Developmental programming: impact of prenatal testosterone excess on steroidal machinery and cell differentiation markers in visceral adipocytes of female sheep. Reprod. Sci. 25 (7), 1010–1023.
Puttabyatappa, M., et al., 2019. Developmental programming: changes in mediators of insulin sensitivity in prenatal bisphenol A-treated female sheep. Reprod. Toxicol. 85, 110–122.
Puttabyatappa, M., et al., 2020. Developmental programming: adipose depot-specific changes and thermogenic adipocyte distribution in the female sheep. Mol. Cell. Endocrinol. 503, 110691.
Ruiz-Ojeda, F.J., et al., 2021. Active integrins regulate white adipose tissue insulin sensitivity and brown fat thermogenesis. Mol. Metabol. 45, 101147.
Russo, R., et al., 2018. Epicardial adipose tissue: new parameter for cardiovascular risk assessment in high risk populations. J. Nephrol. 31 (6), 847–853.
Santos, R.S., et al., 2018. Activation of estrogen receptor alpha induces beiging of adipocytes. Mol. Metabol. 18, 51–59.
Sasaki, N., et al., 2022. Adipose tissue insulin resistance predicts the incidence of hypertension: the Hiroshima study on glucose metabolism and cardiovascular diseases. Hypertens. Res. 45 (11), 1763–1771.
Schaffer, J.E., 2020. Death by lipids: the role of small nucleolar RNAs in metabolic stress. J. Biol. Chem. 295 (25), 8628–8635.
Schleinitz, D., et al., 2020. Identification of distinct transcriptome signatures of human adipose tissue from fifteen depots. Eur. J. Hum. Genet. 28 (12), 1714–1725.
Schoof, E., et al., 2004. Comparison of leptin gene expression in different adipose tissues in children and adults. Eur. J. Endocrinol. 150 (4), 579–584.
Shan, B., et al., 2022. MiR-218-5p affects subcutaneous adipogenesis by targeting ACSL1, a novel candidate for pig fat deposition. Genes 13 (2).
Shen, L., et al., 2016. MicroRNA-23a regulates 3T3-L1 adipocyte differentiation. Gene 575 (2 Pt 3), 761–764.
Shi, T., et al., 2020. Integrated Analysis of miRNA-Mediated ceRNA Networks in Ovine Skeletal Muscle Development. Research Square.
Soronen, J., et al., 2012. Adipose tissue gene expression analysis reveals changes in inflammatory, mitochondrial respiratory and lipid metabolic pathways in obese insulin-resistant subjects. BMC Med. Genom. 5, 9.
Spitzer, M., et al., 2014. BoxPlotR: a web tool for generation of box plots. Nat. Methods 11 (2), 121–122.
Squillaro, T., et al., 2020. Long non-coding RNAs in regulation of adipogenesis and adipose tissue function. Elife 9.
Statello, L., et al., 2021. Gene regulation by long non-coding RNAs and its biological functions. Nat. Rev. Mol. Cell Biol. 22 (2), 96–118.
Stenkula, K.G., Erlanson-Albertsson, C., 2018. Adipose cell size: importance in health and disease. Am. J. Physiol. Regul. Integr. Comp. Physiol. 315 (2), R284–R295.
Tao, L., et al., 2016. Crucial role of miR-433 in regulating cardiac fibrosis. Theranostics 6 (12), 2068–2083.
Tello-Flores, V.A., et al., 2021. Role of long non-coding RNAs and the molecular mechanisms involved in insulin resistance. Int. J. Mol. Sci. 22 (14).
Thomas, H., et al., 2018. Global atlas of cardiovascular disease 2000-2016: the path to prevention and control. Glob. Heart 13 (3), 143–163.
Van Harmelen, V., Rohrig, K., Hauner, H., 2004. Comparison of proliferation and differentiation capacity of human adipocyte precursor cells from the omental and subcutaneous adipose tissue depot of obese subjects. Metabolism 53 (5), 632–637.
van Rooij, E., et al., 2006. A signature pattern of stress-responsive microRNAs that can evoke cardiac hypertrophy and heart failure. Proc. Natl. Acad. Sci. U. S. A. 103 (48), 18255–18260.
Veiga-Lopez, A., et al., 2008. Developmental programming: deficits in reproductive hormone dynamics and ovulatory outcomes in prenatal, testosterone-treated sheep. Biol. Reprod. 78 (4), 636–647.
Veiga-Lopez, A., et al., 2011. Developmental programming: impact of excess prenatal testosterone on intrauterine fetal endocrine milieu and growth in sheep. Biol. Reprod. 84 (1), 87–96.
Veiga-Lopez, A., et al., 2013a. Developmental programming: impact of prenatal testosterone excess on insulin sensitivity, adiposity, and free fatty acid profile in postpubertal female sheep. Endocrinology 154 (5), 1731–1742.
Veiga-Lopez, A., et al., 2013b. Developmental programming: gestational bisphenol-A treatment alters trajectory of fetal ovarian gene expression. Endocrinology 154 (5), 1873–1884.
Veiga-Lopez, A., et al., 2015a. Gender-specific effects on gestational length and birth weight by early pregnancy BPA exposure. J. Clin. Endocrinol. Metab. 100 (11), E1394–E1403.
Veiga-Lopez, A., et al., 2015b. Impact of gestational bisphenol A on oxidative stress and free fatty acids: human association and interspecies animal testing studies. Endocrinology 156 (3), 911–922.
Veiga-Lopez, A., et al., 2016. Developmental programming: interaction between prenatal BPA exposure and postnatal adiposity on metabolic variables in female sheep. Am. J. Physiol. Endocrinol. Metab. 310 (3), E238–E247.
Villasante Fricke, A.C., Iacobellis, G., 2019. Epicardial adipose tissue: clinical biomarker of cardio-metabolic risk. Int. J. Mol. Sci. 20 (23).
Vyas, A.K., et al., 2016. Prenatal programming: adverse cardiac programming by gestational testosterone excess. Sci. Rep. 6, 28335.
Wajahat, M., Bracken, C.P., Orang, A., 2021. Emerging functions for snoRNAs and snoRNA-derived fragments. Int. J. Mol. Sci. 22 (19).
Wang, H., et al., 2017. Anti-androgenic mechanisms of Bisphenol A involve androgen receptor signaling pathway. Toxicology 387, 10–16.
Wang, P.S., Wang, Z., Yang, C., 2021. Dysregulations of long non-coding RNAs - the emerging "lnc" in environmental carcinogenesis. Semin. Cancer Biol. 76, 163–172.
Wei, J.W., et al., 2017. Non-coding RNAs as regulators in epigenetics (Review). Oncol. Rep. 37 (1), 3–9.
Weikard, R., Demasius, W., Kuehn, C., 2017. Mining long noncoding RNA in livestock. Anim. Genet. 48 (1), 3–18.
Xie, H., Lim, B., Lodish, H.F., 2009. MicroRNAs induced during adipogenesis that accelerate fat cell development are downregulated in obesity. Diabetes 58 (5), 1050–1057.
Yamamoto, Y., et al., 2010. Adipose depots possess unique developmental gene signatures. Obesity 18 (5), 872–878.
Ye, Z., et al., 2022. Plasma exosomal miRNAs associated with metabolism as early predictor of gestational diabetes mellitus. Diabetes 71 (11), 2272–2283.

Zarean, M., Poursafa, P., 2019. The role of environmental disruptor chemicals in the development of non communicable disease. Adv. Exp. Med. Biol. 1121, 21–31.
Zhang, Q., et al., 2022. Integrative analysis of multi-omics data to detect the underlying molecular mechanisms for obesity in vivo in humans. Hum. Genom. 16 (1), 15.
Zhao, Y., et al., 2017. MiR-485-5p modulates mitochondrial fission through targeting mitochondrial anchored protein ligase in cardiac hypertrophy. Biochim. Biophys. Acta, Mol. Basis Dis. 1863 (11), 2871–2881.